Geosphere

Controls on the expression of igneous intrusions in seismic reflection data

--Manuscript Draft--

Manuscript Number:	GS1150R1
Full Title:	Controls on the expression of igneous intrusions in seismic reflection data
Short Title:	Imaging intrusions in seismic data
Article Type:	Research Paper
Keywords:	Sill; seismic reflection data; synthetic seismic forward modelling; intrusion
Corresponding Author:	Craig Magee Imperial College London, London UNITED KINGDOM
Corresponding Author Secondary Information:	
Corresponding Author's Institution:	Imperial College
Corresponding Author's Secondary Institution:	
First Author:	Craig Magee
First Author Secondary Information:	
Order of Authors:	Craig Magee
	Shivani Maharaj
	Thilo Wrona
	Christopher A-L Jackson
Order of Authors Secondary Information:	
Abstract:	The architecture of subsurface magma plumbing systems influences a variety of igneous processes, including the physiochemical evolution of magma and extrusion sites. Seismic reflection data provides a unique opportunity to image and analyze these sub-volcanic systems in 3-D and has arguably revolutionized our understanding of magma emplacement. In particular, the observation of (i) interconnected sills, (ii) transgressive sill limbs, and (iii) magma flow indicators in seismic data suggest that sill-complexes can facilitate significant lateral (10's-100's km) and vertical (<5 km) magma transport. However, it is often difficult to determine the validity of seismic interpretations of igneous features because: (i) they are rarely drilled; and (ii) our ability to compare seismically imaged features to potential field analogues is hampered by the limited resolution of seismic data. Here, we use field observations to constrain a series of novel seismic forward models that examine how different sill morphologies may be expressed in seismic data. By varying the geologic architecture (e.g., host rock lithology and intrusion thickness) and seismic properties (e.g., frequency), the models demonstrate that seismic amplitude variations and reflection configurations can be used to constrain intrusion geometry. However, our results also highlight that stratigraphic reflections can interfere with reflections generated at the intrusive contacts, and may thus produce seismic artefacts that could be misinterpreted as real features. This study emphasizes the value of seismic data to understanding magmatic systems and demonstrates the role that synthetic seismic forward modelling can play in bridging the gap between seismic data and field observations.

Controls on the expression of igneous intrusions in seismic reflection data

Craig Magee*, Shivani M. Maharaj, Thilo Wrona, Christopher A-L. Jackson

Basins Research Group (BRG), Department of Earth Science and Engineering,

Imperial College, London, SW7 2BP, UK

**corresponding author e-mail: c.magee@imperial.ac.uk*

Abstract

The architecture of subsurface magma plumbing systems influences a variety of igneous processes, including the physiochemical evolution of magma and extrusion sites. Seismic reflection data provides a unique opportunity to image and analyze these sub-volcanic systems in 3-D and has arguably revolutionized our understanding of magma emplacement. In particular, the observation of (i) interconnected sills, (ii) transgressive sill limbs, and (iii) magma flow indicators in seismic data suggest that sill-complexes can facilitate significant lateral (10's-100's km) and vertical (<5 km) magma transport. However, it is often difficult to determine the validity of seismic interpretations of igneous features because: (i) they are rarely drilled; and (ii) our ability to compare seismically imaged features to potential field analogues is hampered by the limited resolution of seismic data. Here, we use field observations to constrain a series of novel seismic forward models that examine how different sill morphologies may be expressed in seismic data. By varying the geologic architecture (e.g., host rock lithology and intrusion thickness) and seismic properties (e.g., frequency), the models demonstrate that seismic amplitude variations and reflection configurations can be used to constrain intrusion geometry. However, our results also highlight that stratigraphic reflections can interfere with reflections generated at the intrusive contacts, and may thus produce seismic artefacts that could be misinterpreted as real features.

This study emphasizes the value of seismic data to understanding magmatic systems and demonstrates the role that synthetic seismic forward modelling can play in bridging the gap between seismic data and field observations.

1. Introduction

Subsurface networks of igneous intrusions comprise a series of interconnected conduits and reservoirs. The architecture of these systems influences the physiochemical evolution of magma (e.g., Holness and Humphreys, 2003; Magee et al., 2013a), extrusion location (e.g., Gaffney et al., 2007), and the accumulation of economic resources (e.g., Bedard et al., 2012; Holford et al., 2012). Establishing the geometry of individual intrusions and their connectivity is thus crucial to understanding igneous processes. Resolving entire intrusion geometries in the field is, however, hampered by a lack of high-quality, fully three-dimensional exposure and the 2-D nature of the Earth's surface (Fig. 1). Geophysical techniques such as magnetotellurics, InSAR, and reflection seismology have therefore been employed to either constrain subsurface intrusions or track real-time magma migration (e.g., Smallwood and Maresh, 2002; Wright et al., 2006; Biggs et al., 2011; Pagli et al., 2012). Of these techniques, reflection seismology arguably provides the most complete and detailed imaging of individual intrusions and intrusion systems. In particular, intrusions within sedimentary basins can be easily identified and mapped in 2-D and 3-D seismic reflection data due to the large acoustic impedance contrast between igneous rocks and encasing strata (Smallwood and Maresh, 2002). Seismic studies have thus revolutionized our understanding of intrusion systems in sedimentary basins, providing spectacular images of vertically and laterally extensive complexes of strata-concordant and/or saucer-shaped sills (e.g., Fig. 1) (e.g., Symonds et al., 1998; Smallwood and Maresh, 2002; Thomson and Hutton, 2004;

Planke et al., 2005; Polteau et al., 2008; Magee et al., 2013b; Magee et al., 2014a; Sun et al., 2014). Mapping of magma flow indicators in these data has led to an emerging consensus that magma can be transported over significant lateral (up to hundreds of kilometers) and vertical (up to several kilometers) distances via interconnected sills and transgressive inclined sheets (e.g., Cartwright and Hansen, 2006; Magee et al., 2014a). Detailed analyses of these intrusion systems has also shown that: (i) the architecture of magma networks is influenced by the host rock structure, in particular bedding discontinuities and fractures, and lithology (Schofield et al., 2012a; Jackson et al., 2013; Magee et al., 2013c); (ii) igneous activity may be protracted (e.g., incremental intrusion over 15 Myr; Magee et al., 2014a); and (iii) sill-complex construction can impact the distribution and style of host rock deformation (Magee et al., 2014a) and volcanism (Magee et al., 2013d). Constraining the validity of these observations is, however, difficult to accomplish because of the limited vertical and horizontal resolution of seismic reflection data (*c.* ≥ 20 m for igneous rocks) and the lack of boreholes intersecting igneous intrusions.

To help provide a better understanding of the general seismic expression of intrusions, we conduct seismic forward modelling to examine how sill geometries observed in the field are manifested in seismic reflection data. By creating simple geometric geologic models and using real host rock mechanical properties (e.g., Fig. 1), we examine: (i) whether seismic data can be used to determine the connectivity within sill-complexes, i.e. can magma migrate to the surface through a network of sills? (Cartwright and Hansen, 2006); (ii) what inclined sill limbs tell us about magma propagation and emplacement mechanisms; and (iii) the utility of subtle geometric features interpreted in seismic data to constraining magma flow directions. Our results demonstrate that intrusion geometries observed in the field can be this tuning in (synthetic) seismic data. Interference between intrusions and the encasing host rock reflections can, however, generate seismic artefacts that may be misinterpreted.

2. Synthetic Seismic Forward Modelling of Igneous Intrusions

Magmatic bodies are traditionally mapped in seismic data by picking high-amplitude reflections that are considered to correspond to the upper contact between an intrusion and the encasing host rock (Smallwood and Maresh, 2002; Thomson, 2005). Occasionally, underlying high-amplitude reflections are observed that may correlate to the lower intrusive contact (e.g., Hansen and Cartwright, 2006; Jackson et al., 2013). Where both contacts are discernable, the mapped intrusions resemble, at least geometrically, those observed in the field (e.g., Jackson et al., 2013). Most intrusions are, however, expressed as 'tuned' reflection packages (e.g., Fig. 1) (Smallwood and Maresh, 2002). This tuning effect occurs when the vertical intrusion thickness is between the limit of separability and the limit of visibility of the seismic data (sensu Brown, 2004). In this scenario, the reflections emanating from the upper and lower intrusion contact interfere and cannot be distinguished (Widess, 1973; Smallwood and Maresh, 2002; Brown, 2004; Hansen et al., 2008). Although these tuned reflection packages broadly correspond to the 3-D intrusion geometry, the sill thickness can only be estimated to lie between the calculated limits of separability and visibility (e.g., Jackson et al., 2013). The same is true for magma flow indicators, which are typically on the cusp of the vertical seismic resolution (Schofield et al., 2012a). By assessing how pre-defined intrusion morphologies (Fig. 2) are expressed in 2-D seismic reflection data, we aim to examine the validity of seismic-based interpretations concerning the development of intrusion systems and determine if further information can be recovered from real data.

2.1. Modelled intrusion geometries

2.1.1. Large-scale intrusive features and sill connectivity

Field- and seismic-based studies indicate that many magmatic networks within sedimentary basins consist of interconnected, strata-concordant (Fig. 1A) and/or saucer-shaped sills (Fig. 1B) (e.g., Symonds et al., 1998; Smallwood and Maresh, 2002; Thomson and Hutton, 2004; Planke et al., 2005; Polteau et al., 2008). To assess the overall expression of such intrusions in seismic reflection data, we developed a simple 2-D geometric model (Fig. 2A). The model is comprised of a 100 m thick, strata-concordant sill (Sill 1) underlain by a saucer-shaped sill (Sill 2) (Fig. 2A). Because sills commonly taper towards their tips (Hansen and Cartwright, 2006; Hansen et al., 2011), Sill 1 thins laterally (Fig. 2A). The left-hand sill tip thins relatively gradually (top contact dip of 15°) whilst the right-hand termination thins more abruptly (top contact dip of 40°) (Fig. 2A). In contrast, the 100 m thick, strata-concordant portion of Sill 2 transitions laterally into inclined limbs, which dip inwards at 25° (Fig. 2A). This simple framework model provides a context for further examination of the seismic imaging of: (i) connected and unconnected sills; and (ii) inclined sill limbs that either cross-cut a homogeneous or interbedded stratigraphy.

2.1.2. Magma flow indicators

Sheet intrusions, typically, do not initially intrude as bodies of magma with significant along-strike extents (e.g., Rickwood, 1990; Schofield et al., 2012b). Instead, the initial phase of emplacement is commonly dominated by the propagation of thin, discrete ‘magma segments’, which may be vertically and/or laterally offset from each other (Fig. 3) (e.g., Rickwood, 1990; Schofield et al., 2012b). Dependent on the behavior of the host rock during intrusion, the inflation and eventual coalescence of segments as magma input increases can produce a range of structures (e.g., intrusive steps and magma fingers). These flow-related structures are superimposed onto the overall morphology of a continuous sheet intrusion (Fig. 3) (Schofield et al., 2012b). Although there are various magma flow indicators that can be observed in the field, for simplicity, we focus particularly on intrusive steps and magma fingers. Importantly, the long axes of these structures are a proxy for the primary magma flow axis (Fig. 3) (Magee et al., 2012; Schofield et al., 2012b). Identifying types of magma flow indicators can also constrain the syn-emplacement host rock behavior; i.e. intrusive steps occur via brittle fracturing, whereas magma fingers form through non-brittle processes (Pollard et al., 1975; Rickwood, 1990; Hutton, 2009; Schofield et al., 2010; Schofield et al., 2012a; Schofield et al., 2012b).

Mapping magma flow indicators in seismic data, such as intrusive steps and magma fingers (e.g., Figs 1C-D and 3), can thus provide important insights into how melt migrates through a basin and where major magma reservoirs and/or sources reside (Schofield et al., 2010; Schofield et al., 2012a; Schofield et al., 2012b; Magee et al., 2014a). Analyzing flow indicators is also crucial to reconstructing the magmatic history of a sedimentary basin (e.g., Schofield et al., 2012a; Magee et al., 2014a). However, the size of intrusive steps and magma fingers is typically at or below the limit of separability, which means that they are likely to only appear as small vertical offsets and amplitude variations in the mapped reflections (e.g., Figs 1C-D) (Schofield et al., 2012a; Magee et al., 2014a). It can thus be difficult to differentiate the type of magma flow indicator, or if the mapped offsets actually correspond to flow-related structures or if they are simply geophysical artifacts. Because of the uncertainty in the interpretation of magma flow indicators, it is pertinent to assess how such structures are expressed in seismic data.

The models of magma flow indicators represent a cross-section through the inner portion of a centrally fed, saucer-shaped sill and oriented orthogonal to the magma flow direction (Fig. 2B). Figure 2C depicts a series of intrusive steps (Schofield et al., 2012b). It should be noted that, in this model (Fig. 2C), we assume that there are small (20 m), lateral overlaps between each 50 m thick magmatic segment, producing intrusive steps with vertical offsets of 25 m and a local intrusion thickness of 75 m (cf. to geometry shown in Fig. 1C). Figure 2D shows a series of magma fingers, which are elliptical in cross-section when isolated (Schofield et al., 2010; Schofield et al., 2012b), or form a magma lobe upon finger coalescence (Thomson and Hutton, 2004). Magma fingers observed in the field typically have an average height/width aspect ratio of 0.27 (Table. 1); this morphology was incorporated into the model (Fig. 2D). Hypothetical magma fingers with an aspect ratio of 0.65 are also modelled to test how alternate finger geometries may impact seismic expression (Fig. 2D).

2.2. Rock Properties

Seismic forward modelling of igneous intrusions requires attributing realistic physical properties to the igneous rocks and the sedimentary host rocks. In absence of well data, it is commonly assumed that seismically imaged igneous intrusions are basaltic and have a p-wave velocity (V_p) of *c.* 5.55 km s^{-1} and a density (ρ) of *c.* 2.8 g m^3 (Skogly, 1998; Berndt et al., 2000; Bartetzko et al., 2005); we adopt these values in our models (Table. 2). It should be noted that the composition, velocity and density of igneous rocks can vary (e.g., V_p may range from 4–7.5 km s^{-1}; Skogly, 1998; Berndt et al., 2000; Bartetzko et al., 2005). Regardless of potential compositional variations, the V_p of igneous rocks is typically significantly higher than those associated with the sedimentary host rock. The resulting acoustic impedance (density × velocity) contrast between intrusion and sedimentary host rock produces the characteristic high-amplitude reflections.

We derived the physical properties for sandstone and shale host rocks from the porosity, density and elastic moduli of their individual components (water, quartz and smectite, respectively). To create synthetic seismic sections corresponding to a typical depth of 2.5 km, we first derived the host rock porosity (φ) according to Sclater and Christie (1980):

$$\varphi(z) = \varphi_0 e^{-cz}$$

whereby, the porosity depth coefficient (c) is equal to 0.51 km^{-1} for shale and 0.27 km^{-1} for sandstone, assuming that the surface porosity (φ_0) of shale is 0.63 and of sandstone is 0.49. The porosities were then calculated for a typical intrusion depth of 2.5 km (sandstone: 0.25 and shale: 0.18), which is representative of the sub-seabed depths that intrusions occur at in real data. The density (ρ) of sandstone and shale at 2.5 km depth was calculated using averages of grain density (ρ_{grain}) and fluid density (ρ_{fluid}) based on the previously calculated porosities (Table. 2):

$$\rho = \rho_{grain} - \varphi(\rho_{grain} - \rho_{fluid})$$

Density values of 2.24 and 2.19 g cm^{-3} were derived for the sandstone and shale, respectively. We then calculated the corresponding bulk (k) and shear modulus (μ) for each rock type from the elastic moduli of its components and their volume fraction (f_i) (Table. 2). We assumed the pore fluid to be water with a density of 1 g cm^{-3}, a bulk modulus of 2.2 GPa and a shear modulus of zero. Since the shear modulus of water is zero, the Hashin-Shtrikman lower bound can be used to calculate the elastic moduli (Hashin and Shtrikman, 1963) (Table. 2):

$$k^{HS\pm} = k_1 + \frac{f_2}{\frac{1}{k_2 - k_1} + \frac{f_1}{k_1 + \frac{4}{3}\mu_m}}$$

$$\mu^{HS\pm} = \mu_1 + \frac{f_2}{\frac{1}{\mu_2 - \mu_1} + \frac{f_1}{\mu_1 + \frac{\mu_m}{6}\left(\frac{9k_m + 8\mu_m}{k_m + 2\mu_m}\right)}}$$

Note that we adapted the notation of Mavko et al. (2009). Finally, we used the elastic moduli to calculate the p-wave velocity (V_p):

$$V_p = \sqrt{\frac{k + \frac{4}{3}\mu}{\rho}}$$

The resulting values, 1.92 km s^{-1} and 2.03 km s^{-1} for sandstone and shale respectively, are within range of previously reported examples (Jaeger et al. 2009). Bed thicknesses are modelled at either 50 m or 25 m to test how they may impact the expression of igneous intrusions.

2.3. Seismic Modelling

The input models were converted into synthetic seismic section by simulating a zero-offset survey using the Zoeppritz equations and a zero-phase Ricker wavelet typical for seismic forward modelling studies (e.g., Schwab et al., 2007; Holgate et al., 2014; Osagiede et al., 2014). To assess the impact of seismic resolution, which is partially controlled by and, therefore, acts as a proxy for burial depth, on the expression of different intrusions, we varied the wavelet frequency; we chose peak frequencies of 13 Hz, 26 Hz and 45 Hz, which correspond to dominant frequencies of 10 Hz, 20 Hz and 35 Hz (Kallweit and Wood, 1982). Given a V_p of 5.55 km s^{-1} for the intrusions (Skogly, 1998), these frequencies can also be used to determine the limits of separability and visibility expected for the synthetic seismic data (Fig. 4). To assess the 'ideal' seismic expression of different intrusion geometries using synthetic seismic forward modelling, parameters that are likely to further degrade the seismic imaging quality are not accounted for. These include such as seismic noise and depth-dependent amplitude and frequency decay. The imaging beneath the modelled intrusions is therefore of relatively high-quality, whereas a marked drop in reflection continuity and amplitude may be expected in real data (e.g., Hansen et al., 2008).

3. Seismic expression of sills

It is apparent from Figures 5 and 6 that the expression of intrusions in synthetic seismic data geometrically resembles the input models, particularly those that only incorporate a homogeneous sandstone host rock. In the 45 Hz, homogeneous host rock model, the sills display constant, moderate amplitudes when the intrusion thickness exceeds 51 m (Fig. 5B). Figure 5B shows that as the thickness decreases, constructive interference between the upper and lower contact reflections produces an increase in amplitude, which peaks at the limit of separability for the data (i.e. 31 m; Fig. 4). A continued decrease in intrusion thickness below the limit of separability corresponds to a reduction in the degree of constructive interference and a transition into destructive interference (Fig. 5B). This variation in the degree of interference is demarcated by decrease in amplitude (Fig. 5B). The 'humped' amplitude profile geometries characteristic of seismic interference between two lithological boundaries (Widess, 1973; Hansen et al., 2008) are developed at the lateral terminations of each sill (Fig. 5B). Amplitude variations are also observed in the basal Sill 1 and top Sill 2 reflections immediately adjacent to the sill-sill junction, which is characterized by a break in reflection continuity (Fig. 5B).

Similar amplitude profiles are associated with the sills in the 26 Hz, homogeneous sandstone host rock model (Fig. 5C). The sill junction is, however, more complex; the basal Sill 1 reflection and top Sill 2 reflection appear to extend upwards into the package that defines Sill 1 (Fig. 5C). Within the 13 Hz, homogeneous sandstone host rock model, the ≤100 m thick sills (Fig. 2A) are below the limit of separability (i.e. 107 m; Fig. 4); there is thus no constructive interference or presence of 'humped' amplitude profiles towards the sill margins, but simply a reduction in amplitude where the intrusion thickness decreases further below the limit of separability (Fig. 5D). Complexity occurs at the sill junction, where the cumulative intrusion thickness locally increases to 175 m (Fig. 5D). In this location, a subdued increase in amplitude is observed to the left of the junction along the top Sill 2 reflection. The width of the poorly resolved connection is, however, characterized by abrupt decreases and increases in amplitude, particularly along the basal Sill 1 reflection (Fig. 5D).

In comparison to those models containing a homogeneous host rock, Figure 6 highlights the influence that a heterogeneous host rock has on the seismic expression of the sills. In all models, the inclined limb reflections, which cross-cut stratigraphy, appear to have a stepped morphology despite being planar (Fig. 6). Because these step-like structures are not related to magma propagation (cf. Fig. 3) (cf. Schofield et al., 2012b), we refer to them as 'pseudo-steps'. The pseudo-step geometry is most pronounced at lower frequencies (i.e. 13 Hz; Fig. 6D), where it is clear that they correlate to abrupt fluctuations in amplitude.

3.1. Resolvability of sill connectivity

By examining the expression of sill junctions in detail (Fig. 7), we aim to establish whether amplitude variations or reflection geometries may be used to determine the connectivity of a sill-complex. So that we are isolating the impact of sill connectivity and not, for example, imaging amplitude variations associated with a heterogeneous host rock, we only use a homogeneous sandstone host rock. The connected sills within the 45 Hz model are distinguished by a break in the basal Sill 1 reflection (Fig. 7B). However, when the two sills are separated by 10 m or 50 m, the basal Sill 1 reflection is continuous (Figs 7F and J). In each 45 Hz model, the amplitude of the top Sill 2 reflection increases as it approaches Sill 1

(Figs 7B, F and J). Amplitude variations are only observed along the basal Sill 2 reflection when a gap between the two sills is present (Figs 7F and J) and not when the sills are connected (Fig. 6B). At 26 Hz (Figs 6C, G and K), and particularly at 13 Hz (Figs 7D, H and L), the detail of the sill junction becomes harder to resolve. Figures 7D, H and L highlight that the top reflection of Sill 1 in the 13 Hz models, denoted by a yellow line, is more perturbed when the two sills are connected. Although only three of the generated seismic sections correspond to a connected sill (i.e. Figs 7B-D), most of the synthetic reflection configurations, perhaps with the exception of Figure 7J, appear to resemble sill-sill junctions.

3.2. Seismic expression of inclined limbs

Pseudo-steps occur in the seismic sections of planar inclined limbs encased by an interbedded host rock stratigraphy regardless of frequency, although they are more prominent at lower frequencies (Figs 5, 6 and 8). Figures 8H and L demonstrate that the lateral extent of individual pseudo-steps decreases as bed thickness decreases. A similar decrease in the lateral extent of pseudo-steps occurs in response to a reduction in inclined limb thickness (Figs 8H and P). In addition to the abrupt changes in amplitude associated with pseudo-steps, the ‘apparent thickness’ of an intrusion (i.e. the vertical distance between the maximum peak and trough positions of the prominent top and basal reflections) varies with respect to the vertical thickness of the input model (Fig. 8). For example, the apparent thickness measured at the top-left termination of each inclined limb is greater than the vertical thickness of the input models (Fig. 8). Within individual models, across the rest of the intrusion, regardless of whether the top and base reflections are discretely defined, the apparent thickness appears to fluctuate (Fig. 8). In some instances the apparent thickness decreases below the vertical thickness of the input model (e.g., Figs 8F, G, H, N and O), although most seismograms demonstrate that apparent thicknesses greater than the vertical thickness of the input model is dominant. Despite all synthetic seismograms modelled with a heterogeneous host rock stratigraphy displaying variations in both apparent thickness and amplitude, there appears to be no systematic relationship between the two measured parameters. Several observations are, however, worth highlighting: (i) the apparent thickness of the inclined limb is greater than the vertical thickness of the input model (i.e. 75 m) for all synthetic seismograms generated from Figure 8I where the bed thickness is only 25 m (i.e. Figs 8J, K and L); (ii) maxima in the amplitude of top reflection in Figure 8L correspond to increases in apparent thickness; and (iii) conversely, peaks in apparent thickness along the inclined limb in Figure 8K correlated to amplitude minima.

3.3. Resolving magma flow indicators

3.3.1. Intrusive steps

Within a homogeneous host rock, intrusive steps are easily recognizable and the only fluctuations in amplitude occur at the magmatic segment connections (Figs 9B-D). Reducing the frequency of the data produces an increase in apparent thickness of the intrusion (Figs 9B-D). The presence of a heterogeneous host rock stratigraphy, with beds parallel to the modelled intrusive segments, alters the seismic expression of the sill (Figs 9E-L). Depending on the bed thickness and the position of the segments relative to the different host rock lithologies (i.e. whether segments are immediately overlain by sandstone or shale), there are significant variations in: (i) the amplitude of each magmatic segment in individual models, with some segments seeming to 'blend' into the background stratigraphic reflections (e.g., Figs 9F-H); (ii) the apparent thickness of individual segments (e.g., Fig. 9H); and (iii) the vertical offset, or step height, between segments (e.g., Fig. 9K).

3.3.2. Magma fingers

Across all the models there are prominent variations in amplitude along the top and basal magma finger reflections, which spatially correlate to changes in the actual and apparent intrusion thickness (Fig. 10). Within homogeneous host rocks the true geometry of the magma fingers becomes less recognizable with a decrease in frequency, particularly for those with a higher aspect ratio (Figs 10B-D). The resolvability of magma finger geometries is further compounded by the addition of alternating sandstone and shale beds (Fig. 10). For example, the basal reflection of the magma fingers expressed in Figure 10H have a more prominent curvature than that of the top magma finger reflection. In Figure 10P it is the top magma finger reflection that displays a greater curvature. In both of these examples, the contact reflection displaying the greater curvature is primarily hosted by shale beds (Figs 10H and P). From the models presented in Figures 10H and P, it is also difficult to discern the high-aspect ratio magma fingers from the background stratigraphic reflections. Where the magma fingers cross-cut lithological boundaries, the synthetic seismic reflections corresponding to the host rock strata appear to onlap onto or are truncated by the intrusion.

4. Discussion

Whilst seismic data has revolutionized our understanding of magma plumbing systems within sedimentary basins, we rely upon qualitative visual comparison with field analogues to interpret the origin of intrusion morphologies imaged. For example, sill-sill junctions, subtle inclined limb geometries and magma flow indicators, all of which are key to elucidating the connectivity and emplacement of entire sill-complexes, are interpreted in seismic data based on field analogues. There are, however, two key problems associated with qualitative comparisons between seismic and field data: (i) seismic data is restricted in its resolution, such that smaller scale (typically <10–20 m) structures are not fully resolved; and (ii) the 3-D geometry of intrusions exposed in the field is commonly limited. By demonstrating that synthetic seismograms can generally reproduce the geometry of the input intrusion models, which incorporate a variety of field observations, our results represent an important first step in bridging the resolution gap between seismic and field data (Figs 5-10).

In this section, we discuss the implications of our results in light of how the synthetic seismic produced relates to both real seismic and field examples. Overall, if the host rock is homogeneous, individual intrusion geometries are particularly well defined (e.g., Fig. 5). In these models it is apparent that variations in the amplitude profiles correspond to interference between the upper and lower contact reflections (Fig. 5). This tuning response occurs below the limit of separability and is a function of the intrusion thickness and frequency content of the seismic data (Widess, 1973; Smallwood and Maresh, 2002). The seismic expression (i.e. geometry and amplitude) of different intrusions may vary in response to changes in the frequency, the thickness of the intrusion, and the presence of interbedded strata (Figs 5 and 6). Addition of a heterogeneous host rock stratigraphy complicates the seismic expression, i.e. the reflection configuration and amplitude, of igneous intrusions. These affects are considered in more detail below.

4.1. Can seismic data be used to determine connectivity in sill-complexes?

Extensive sill-complexes have been recognized in a variety of sedimentary basins (e.g., Karoo Basin, South Africa, Chevallier and Woodford, 1999; the Vøring and Møre basins, offshore Norway, Cartwright and Hansen, 2006; South Yellow Sea Basin, offshore China, Lee et al., 2006; offshore NW Australia, Rohrman, 2013; Rockall Basin, NE Atlantic, Magee et al., 2014a). In seismic data, these intrusion systems consist primarily of strata-concordant and/or saucer-shaped sills (Cartwright and Hansen, 2006), which appear to be connected via a range of sill junctions (e.g., Fig. 7A) (Hansen et al., 2004; Thomson and Hutton, 2004).

Although these junctions can also form in response to sill abutment and, thus, may not be indicative of through-going magma flow pathways (Hansen et al., 2004; Thomson and Hutton, 2004; Galerne et al., 2011), sill-complexes are typically considered to transport magma over significant lateral and vertical distances through the upper crust (e.g., Cartwright and Hansen, 2006; Svensen et al., 2012; Magee et al., 2014a). However, limited seismic resolution and a paucity of field exposures mean that the assumed connectivity of entire sill-complexes can rarely be physically confirmed. Assessing the degree of connectivity between sills is crucial to understanding whether sill-complexes can facilitate extensive lateral and vertical magma transport. This is important because mechanisms of magma migration in sedimentary basins can influence: (i) volcano distributions (Magee et al., 2013d); (ii) magma fractionation and contamination; and (iii) compartmentalization of fluids (Holford et al., 2012; Holford et al., 2013).

The modelled seismic expression of a junction between a strata-concordant sill and an underlying saucer-shaped sill reveals that the continuity and amplitude of intrusion-related reflections is sensitive to the frequency of the data (Figs 5-7). Within synthetic models with higher frequency contents, where the sill contacts are clearly resolved, the presence of gaps between the two intrusions can be inferred from the continuity of the lower Sill 1 reflection (Figs 7B, F and J). Importantly, our results highlight that slivers of host rock between the two intrusions, particularly when modelled with low frequencies (e.g., Fig. 7H), could easily be misinterpreted as a fully connected, sill-feeding-sill relationship (cf. Fig. 7D). However, there are several nuances in the imaging of the sill junction zone that may allow connectivity to be assessed. For example, there is a greater deflection in the peak wavelet position of the Sill 1 tuned reflection package where the intrusions are connected (i.e. denoted by a yellow line in Fig. 7D) compared to those separated by host rock (Figs 7H and L). Figure 11 presents a real seismic example of a sill (i.e. Sill A) from the Rockall Basin, offshore NW Ireland, whereby a deflection in the peak wavelet position and a significant decrease in amplitude correspond to an inferred junction with the underlying Sill B. Although it is difficult to determine whether this narrow zone of low amplitude and peak wavelet deflection in Sill A corresponds to an intrusive step or not, the close proximity to and inferred trajectory of the underlying Sill B bears a similarity to Figure 7D and suggests that sills A and B are connected (Fig. 11). However, Figure 11 does highlight one issue with real seismic data, in that imaging immediately beneath a sill is typically poor due to the attenuation of energy in the intrusion. By determining the frequency content of the seismic data and analyzing variations in reflection configurations for a series of imaged sill junctions, it may be possible to establish connectivity across a sill-complex. Interpreted connections could be tested by mapping magma flow indicators, if present, to see if sills were fed from identified connections.

4.2. What do inclined limbs tell us about magma emplacement mechanisms?

Inclined limbs provide important magma flow pathways in sill-complexes, facilitating magma ascent through significant thicknesses (e.g., 2 km) of sedimentary strata (Thomson and Hutton, 2004; Cartwright and Hansen, 2006; Magee et al., 2013b; Magee et al., 2014a). Distinguishing whether emplacement of these limbs occurred via either the passive or forceful intrusion of magma intrusion is important because these mechanisms can result in different styles of host rock deformation, and thereby potentially control surrounding fluid flow (e.g., of hydrothermal fluids or hydrocarbons). For example, the forceful intrusion of magma is typically considered to be associated with the development of new fracture sets (e.g., Rubin, 1995), which may locally increase the permeability of the host rock. Conversely, passively emplaced limbs are likely to exploit pre-existing fractures and fractures (e.g., Magee et al., 2012), potentially forming baffles to subsequent fluid flow or influencing later fault reactivation (Holford et al., 2012; Holford et al., 2013; Magee et al., 2014b).

Furthermore, identifying whether magma exploits pre-existing faults or fractures can provide important insights into the distribution of volcanoes (Gaffney et al., 2007).

A number of mechanisms, which can be sub-divided into those resulting from either the passive or the forceful intrusion of magma, have been proposed to explain inclined limb formation: (i) emplacement of magma into tensile fractures generated by extensional strains applied to the host rock during intrusion-induced forced folding (Fig. 12A) (Thomson and Schofield, 2008; Galland and Scheibert, 2013; Magee et al., 2013c; Magee et al., 2014a); (ii) exploitation of reverse faults instigated by overburden uplift (Fig. 12B) (Thomson and Schofield, 2008); (iii) intrusion along pre-existing faults (Fig. 12C) (Bedard et al., 2012; McClay et al., 2013; Magee et al., 2014b) ; or (iv) forceful transgression of a sub-horizontal sill, hosted within a homogeneous elastic media, in response to asymmetrical stress fields generated during emplacement (Fig. 12D) (Malthe-Sørenssen et al., 2004). The first three mechanisms commonly produce relatively planar inclined limbs in cross-section (e.g., Fig. 2A) (e.g., Thomson and Schofield, 2008; Magee et al., 2013b), whereas numerical modelling suggests that transgression induced by stress field variations results in an inclined limb with a stepped morphology (e.g., Fig. 2C) (Malthe-Sørenssen et al., 2004). Malthe-Sørenssen et al. (2004) provide a real seismic example of a sill offshore NW Australia with stepped inclined limbs, which they use to support their numerical modelling.

Our models demonstrate that planar inclined limbs, which cross-cut stratigraphy, may appear to consist of prominent strata-concordant steps in seismic reflection data (Figs 6 and 8). Figures 13A-C illustrate that these steps are a geophysical artefact, which we refer to as ‘pseudo-steps’, generated by the interference between the sill and cross-cut bedding reflections. This cross-cutting relationship between the sill and stratigraphy effectively produces a series of ‘tuning wedges’ between the two interfaces (Fig. 13A) (cf. Widess, 1973; Brown, 2004). When the vertical thickness of each wedge decreases below the limit of separability of the data, the corresponding sill reflection is pulled-up or pushed-down relative to its actual position (Fig. 13C). This tuning effect also superimposes abrupt increases or decreases in amplitude and apparent intrusion thickness along the length of the inclined limb (Fig. 13). Figure 14A documents a real example from a 3-D seismic dataset located in the Rockall Basin, offshore NW Ireland, whereby subtle changes in the dip of the inclined limb imaged: (i) coincide with reductions in amplitude; and (ii) approximately correlate to intersections between prominent stratigraphic horizons. Whilst it is difficult to fully ascertain the true geometry of igneous intrusions expressed by tuned reflections, we suggest that the inclined limb imaged in Figure 14B is actually planar, based on comparison to synthetic seismic models of sills observed in the field.

Although the arrangement of the intrusive steps in Figure 8 was designed to test the seismic expression of magma flow indicators, the model configuration may also be considered similar to that of the stepped inclined limbs modelled by Malthe-Sørenssen et al. (2004) (Fig. 12D). In contrast to the planar inclined limb modelled in Figures 5, 6 and 8, inclined limbs that originally have a stepped morphology and cross-cut stratigraphy (i.e. Figs 2C and 9) appear to consist of discrete, geometric segments with apparently different properties (e.g., apparent thickness, amplitude and vertical offset). The expression of these segments is dependent on their position and actual thickness relative to bedding (Fig. 9). Such variations in the apparent thickness, amplitude and vertical offset of inclined limbs, however, have not been reported in seismic reflection studies. It is therefore possible that the natural example of apparently stepped inclined limbs from offshore NW Australia, provided by Malthe-Sørenssen et al. (2004) to support their numerical model, may actually represent a planar inclined limb emplaced passively. This challenges models suggesting inclined sill limbs are forcefully emplaced (cf. Malthe-Sørenssen et al., 2004). Numerical modelling of sill transgression in a layered medium, as opposed to a homogeneous host rock (Malthe-

Sørenssen et al., 2004), and further comparison to seismic and field examples is required to test this implication of our results. In particular, analyzing the geometry of the wavelet across an inclined limb may allow interference between inclined limb and host rock reflections to be distinguished (Fig. 13C).

4.3. Can subtle geometric features be interpreted as magma flow indicators?

Figures 9 and 10 indicate that magma flow indicators can be discerned in seismic reflection data. However, their original morphology may be difficult to distinguish depending on the frequency of the seismic data and the thickness and composition of strata truncated by the intrusion (Figs 9 and 10). For example, the variable expression of intrusive steps in the synthetic seismic sections is discussed above (Fig. 9). Comparing our results in Figure 9 to the intrusive steps imaged in Figure 1C, we suggest that the real example constitutes a sill within a thinly bedded or host rock (cf. Figs 9K and L). A thinly bedded host rock, relative to the intrusion thickness, would explain the consistently higher amplitudes of the sill imaged in Figure 1C relative to the host rock. However, we note that the actual vertical offset of the steps is difficult to evaluate (Fig. 1C). It is clear that the apparent morphology of magma fingers in seismic data can vary greatly. Magma fingers hosted in homogeneous host rock and imaged in high frequency data may be well resolved (Fig. 10). In contrast, interference with bedded stratigraphy, particularly at lower frequencies, causes the magma fingers to (Fig. 10): (i) have a conical appearance if they have a low aspect ratio; and (ii) 'blend' in with the background stratigraphy if their aspect ratio is relatively high. The apparent onlap onto the magma fingers or truncation of underlying reflections (Fig. 10), produced by the intrusion of stratigraphic horizons by the intrusion, may mean that they are misinterpreted as extrusive features such as eye-shaped hydrothermal vents (e.g., Hansen, 2006; Magee et al., 2015).

Although our results suggest magma flow indicators can be interpreted, albeit with caution, constraining the seismic frequency and the relative bed thickness can help improve certainty.

5. Conclusions

We present a series of synthetic seismic forward models that examine how igneous intrusions observed in the field may be expressed in seismic reflection data. Our results demonstrate that the appearance of intrusions in seismic data is controlled by a range of parameters, including the intrusion thickness, frequency of the data, and the style of the host rock (i.e. whether it is homogeneous or interbedded). Whilst the majority of the modelled geometries are relatively well defined in synthetic seismograms, geophysical artefacts generated by the interference between intrusive contact and bedding plane reflections can impact image quality and, thereby, interpretations. These issues particularly arise when the size of the intrusive structures imaged (e.g., sill-sill connections or magma flow indicators) are on the cusp of or below the limit of separability. The broad correlation between field observations and synthetic seismic models strengthens the importance of seismic reflection data to the study of igneous systems and suggests seismic forward modelling provides a useful method for testing interpretations.

Acknowledgements

Ikon Geoscience is thanked for providing the synthetic seismic forward modelling software and continued technical support. We are grateful to Geoscience Australia for seismic data provision and to Schlumberger for seismic interpretation software. Katarina Roele is thanked for conducting initial tests on the synthetic seismic forward modelling of intrusions. Shanaka de Silva is thanked for the editorial handling of the paper and Craig Jones and two anonymous reviewers are thanked for their constructive reviews.

Figure Captions

Figure 1: Field analogues to intrusion morphologies interpreted from seismic reflection data. (A) Strata-concordant sills observed in the Bight Basin offshore southern Australia (seismic example) and the Theron Mountains in Antarctica (field example; photo courtesy of Prof. Donny Hutton). (B) Seismic images of a saucer-shaped sill in 3-D and cross-section (modified from Magee et al., 2013c) and an oblique view of the Golden Valley Sill exposed in the Karoo Basin, South Africa (image from Google Earth). (C) A 3-D view of intrusive steps with long axes oriented parallel to the dip direction of the inclined sill limb (see also Magee et al., 2013b) and an orthogonal cross-section from a sill located in the Exmouth Sub-basin offshore NW Australia (seismic example). The field photo is of a sill exposed on Axel Heiberg Island in the Sverdrup Basin of Arctic Canada (courtesy of Prof. Martin Jackson). (D) Magma fingers from a sill in the Rockall Trough (modified from Thomson and Hutton, 2004) and the Golden Valley Sill, South Africa. In the three seismic sections, VE corresponds to ‘vertical exaggeration’ and the measured time in seconds is two-way travel time.

Figure 2: Synthetic seismic input models based on field observations of igneous intrusions (e.g., Fig. 1). (A) A strata-concordant sill (Sill 1) underlain by and connected to a saucer-shaped sill (Sill 2). (B) Schematic map-view of Sill 2. Dotted lines (contours) and the dark-to-light red color gradient emphasize that the lateral margin of Sill 2 transgresses upwards to form an inclined limb around a horizontal inner sill (cf. Thomson and Hutton, 2004). (C and D) Cross-sections through different magma flow indicators (see Fig. 2B for locations) (based on Schofield et al., 2012b): (C) intrusive steps (e.g., Fig. 1C); and (D) magma fingers, which

are either isolated or have coalesced. The 0.27 aspect ratios of the magma fingers is based on field data (Table. 1), whilst the fingers with a 0.65 aspect ratio have been modelled to test how a different magma finger geometry may be expressed in seismic data.

Figure 3: Schematic diagrams depicting how intrusive steps (A) and magma fingers (B), form and can be used to infer magma flow axes (based on Schofield et al., 2012b).

Figure 4: Plot of peak frequency versus intrusion thickness, highlighting the parameter combinations required to: (i) resolve both the top and basal sill contacts; and (ii) produce a tuned reflection package. Below the limit of visibility, particularly if noise were added to the models, no reflections could confidently be assigned to an intrusion (after Osagiede et al., 2014). The three peak frequencies used in this study are also shown.

Figure 5: Synthetic seismograms imaging two connected sills (Fig. 2A) encased by a homogeneous sandstone host rock. Each seismic section is presented in depth and plots of reflection amplitude across the sills are also displayed. As the frequency of the synthetic data increases, the resolvability of the sill contacts decreases. Changes in the amplitude of the top and basal sill contacts relative to the intrusion thickness and limit of separability are shown.

Figure 6: Synthetic seismograms examining the seismic expression of the two connected sills imaged in Figure 4 if the host rock consists of interbedded (50 m bed thickness) sandstone and shale. The mechanical contrast is modelled as either high (B-D) or low (F-H) to assess the impact of heterogeneity on the intrusions. Amplitude plots for each model reveal that there are a series of perturbations in amplitude compared to the homogenous host rock

models (cf. Fig. 5); these variations in amplitude correspond to ‘pseudo-steps’ in the inclined limbs of Sill 2. See Figure 2 for a key to the input models.

Figure 7: Three models testing the seismic expression of the junction zone between sills 1 and 2 if they are connected (A-D) or separated by gaps of 10 m (E-H) and 50 m (I-L) (see Fig. 2A for location). In the 13 Hz models (D, H and L), the position of the wavelet peak corresponding to the Sill 1 tuned reflection package is highlighted by a thin yellow line.

Figure 8: Zoomed in sections of the left-hand inclined limb of Sill 2 (see Fig. 2A), which test the influence of interbedded sandstone and shale on the generation of apparent steps (‘pseudo-steps’) in the seismic expression of the intrusion. Both bed thickness and limb thickness are varied. The 25 m thick beds are barely resolved in the 13 Hz models (L, and P) because they are below the limit of visibility (Fig. 4). The graphs also incorporate the relative difference between the modelled intrusion thickness and the apparent thickness measured from the synthetic seismic data (grey shaded areas).

Figure 9: Synthetic seismograms corresponding to intrusive steps (Fig. 2C). For simplicity, only the amplitude of the reflection peak (blue) is plotted.

Figure 10: Synthetic seismograms of magma fingers (Fig. 2D). Magma fingers with aspect ratios of 0.27 and 0.65 are modelled; for each aspect ratio, one finger is isolated and the others are coalesced (i.e. a magma lobe). Because it is clear that the interbedded host rock significantly influences the seismic expression of the magma fingers, the right-hand models (M-P) contain a ‘reversed’ stratigraphy.

Figure 11: An example of a junction between an overlying strata-concordant sill and an underlying inclined sheet observed in seismic data from the Rockall Basin, offshore NW Ireland (see Magee et al., 2014a). Note that the inferred connection site corresponds to an undulation in and significant amplitude decrease of the Sill A reflection.

Figure 12: Schematic models showing the evolution of inclined limbs via: (A) intrusion of tensile fractures produced during forced folding (after Thomson and Schofield, 2008); (B) intrusion of a reverse fault formed to accommodate roof uplift (after Thomson and Schofield, 2008); (C) exploitation of a pre-existing fault (after Magee et al., 2013b); and (D) formation of, and intrusion along, new fractures in areas of locally increased stress (dashed circles) (Malthe-Sørenssen et al., 2004). (A-C) are typically considered as passive emplacement mechanisms whereas (D) requires forceful intrusion of magma.

Figure 13: Comparison between the input model (A) and seismic expression (B) of an inclined limb that cross-cuts stratigraphy. This configuration produces a series of 'tuning wedges' (Widess, 1973) above and below the inclined limb. The limb thickness is 75 m and the bed spacing is 50 m. (C) Wiggle traces of the synthetic seismogram overlain by the input model highlight areas where the peak and trough of the tuned reflection package (yellow line) deviates from the expected position (i.e. that of the modelled limb).

Figure 14: (A) An inclined sill limb potentially displaying pseudo-steps observed in seismic data from the Rockall Basin, offshore NW Ireland (see Sill 21, Figure 3C of Magee et al., 2014a). (B) Planar inclined limb of the Golden Valley Sill, South Africa.

References

Bartetzko, A., Delius, H., and Pechnig, R., 2005, Effect of compositional and structural variations on log responses of igneous and metamorphic rocks. I: mafic rocks, *in* Harvey, P. K., Brewer, T. S., Pezard, P. A., and Petrov, V., eds., Petrophysical Properties of Crystalline Rocks, Volume 240, Geological Society, London, Special Publications, p. 255-278.

Bedard, J. H., Naslund, H. R., Nabelek, P., Winpenny, A., Hryciuk, M., Macdonald, W., Hayes, B., Steigerwaldt, K., Hadlari, T., Rainbird, R., Dewing, K., and Girard, E., 2012, Fault-mediated melt ascent in a Neoproterozoic continental flood basalt province, the Franklin sills, Victoria Island, Canada: Geological Society of America Bulletin, v. 124, no. 5-6, p. 723-736.

Berndt, C., Skogly, O., Planke, S., Eldholm, O., and Mjelde, R., 2000, High-velocity breakup-related sills in the Vøring Basin, off Norway: Journal of Geophysical Research: Solid Earth (1978–2012), v. 105, no. B12, p. 28443-28454.

Biggs, J., Bastow, I. D., Keir, D., and Lewi, E., 2011, Pulses of deformation reveal frequently recurring shallow magmatic activity beneath the Main Ethiopian Rift: Geochemistry, Geophysics, Geosystems, v. 12, no. 9, p. Q0AB10.

Brown, A. R., 2004, Interpretation of three-dimensional seismic data, Oklahoma, USA, AAPG and SEG, AAPG Memoir 42, SEG Investigations in Geophysics No. 9, 534 p.:

Cartwright, J., and Hansen, D. M., 2006, Magma transport through the crust via interconnected sill complexes: Geology, v. 34, no. 11, p. 929-932.

Chevallier, L., and Woodford, A., 1999, Morpho-tectonics and mechanism of emplacement of the dolerite rings and sills of the western Karoo, South Africa: South African Journal of Geology, v. 102, no. 1, p. 43-54.

Gaffney, E. S., Damjanac, B., and Valentine, G. A., 2007, Localization of volcanic activity: 2. Effects of pre-existing structure: Earth and Planetary Science Letters, v. 263, no. 3, p. 323-338.

Galerne, C. Y., Galland, O., Neumann, E.-R., and Planke, S., 2011, 3D relationships between sills and their feeders: evidence from the Golden Valley Sill Complex (Karoo Basin) and experimental modelling: Journal of Volcanology and Geothermal Research, v. 202, no. 3-4, p. 189-199.

Galland, O., and Scheibert, J., 2013, Analytical model of surface uplift above axisymmetric flat-lying magma intrusions: Implications for sill emplacement and geodesy: Journal of Volcanology and Geothermal Research, v. 253, p. 114-130.

Hansen, D. M., Cartwright, J. A., and Thomas, D., 2004, 3D seismic analysis of the geometry of igneous sills and sill junction relationships, *in* Davies, R. J., Cartwright, J., Stewart, S. A., Lappin, M., and Underhill, J. R., eds., 3D seismic technology: Application to the Exploration of Sedimentary Basins, Volume 29, Geological Society, London, Special Publications, p. 199-208.

Hansen, D. M., and Cartwright, J., 2006, The three-dimensional geometry and growth of forced folds above saucer-shaped igneous sills: Journal of Structural Geology, v. 28, no. 8, p. 1520-1535.

Hansen, D. M., 2006, The morphology of intrusion-related vent structures and their implications for constraining the timing of intrusive events along the NE Atlantic margin: Journal of the Geological Society, v. 163, p. 789-800.

Hansen, D. M., Redfern, J., Federici, F., di Biase, D., and Bertozzi, G., 2008, Miocene igneous activity in the Northern Subbasin, offshore Senegal, NW Africa: Marine and Petroleum Geology, v. 25, no. 1, p. 1-15.

Hansen, J., Jerram, D., McCaffrey, K., and Passey, S., 2011, Early Cenozoic saucer-shaped sills of the Faroe Islands: an example of intrusive styles in basaltic lava piles: Journal of the Geological Society, v. 168, no. 1, p. 159-178.

Hashin, Z., and Shtrikman, S., 1963, A variational approach to the theory of the elastic behaviour of multiphase materials: Journal of the Mechanics and Physics of Solids, v. 11, no. 2, p. 127-140.

Holford, S. P., Schofield, N., MacDonald, J. D., Duddy, I. R., and Green, P. F., 2012, Seismic analysis of igneous systems in sedimentary basins and their impacts on hydrocarbon prospectivity: examples from the southern Australian margin: APPEA Journal, v. 52, p. 23.

Holford, S. P., Schofield, N., Jackson, C. A. L., Magee, C., Green, P. F., and Duddy, I. R., 2013, Impacts of igneous intrusions on source and reservoir potential in prospective sedimentary basins along the western Australian continental margin, *in* Keep, M., and Moss, S. J., eds., The Sedimentary Basins of Western Australia IV: Perth, WA, Proceedings of the Petroleum Exploration Society of Australia Symposium.

Holgate, N. E., Hampson, G. J., Jackson, C. A., and Petersen, S. A., 2014, Constraining uncertainty in interpretation of seismically imaged clinoforms in deltaic reservoirs, Troll Field, Norwegian North Sea: Insights from forward seismic models of outcrop analogs: AAPG Bulletin, no. 20,140,710.

Holness, M., and Humphreys, M., 2003, The Traigh Bhàn na Sgùrra sill, Isle of Mull: Flow localization in a major magma conduit: Journal of Petrology, v. 44, no. 11, p. 1961-1976.

Hutton, D. H. W., 2009, Insights into magmatism in volcanic margins: bridge structures and a new mechanism of basic sill emplacement - Theron Mountains, Antarctica: Petroleum Geoscience, v. 15, no. 3, p. 269-278.

Jackson, C. A.-L., Schofield, N., and Golenkov, B., 2013, Geometry and controls on the development of igneous sill–related forced folds: A 2-D seismic reflection case study from offshore southern Australia: Geological Society of America Bulletin, v. 125, no. 11-12, p. 1874-1890.

Kallweit, R., and Wood, L., 1982, The limits of resolution of zero-phase wavelets: Geophysics, v. 47, no. 7, p. 1035-1046.

Lee, G. H., Kwon, Y. I., Yoon, C. S., Kim, H. J., and Yoo, H. S., 2006, Igneous complexes in the eastern Northern South Yellow Sea Basin and their implications for hydrocarbon systems: Marine and Petroleum Geology, v. 23, no. 6, p. 631-645.

Magee, C., Stevenson, C., O'Driscoll, B., Schofield, N., and McDermott, K., 2012, An alternative emplacement model for the classic Ardnamurchan cone sheet swarm, NW Scotland, involving lateral magma supply via regional dykes: Journal of Structural Geology, v. 43, no. 0, p. 73-91.

Magee, C., O’Driscoll, B., Petronis, M. S., Stevenson, C. T. E., Clay, P. L., and Gertisser, R., 2013a, Magma Rheology Variations in Sheet Intrusions of the Ardnamurchan Central Complex (Scotland) Inferred from Gabbro Inclusion Characteristics: Journal of Petrology, v. 54, no. 1, p. 75-102.

Magee, C., Jackson, C. A.-L., and Schofield, N., 2013b, The influence of normal fault geometry on igneous sill emplacement and morphology: Geology, v. 41, no. 4, p. 407-410.

Magee, C., Briggs, F., and Jackson, C. A.-L., 2013c, Lithological controls on igneous intrusion-induced ground deformation: Journal of the Geological Society, v. 170, no. 6, p. 853-856.

Magee, C., Hunt-Stewart, E., and Jackson, C. A. L., 2013d, Volcano growth mechanisms and the role of sub-volcanic intrusions: Insights from 2D seismic reflection data: Earth and Planetary Science Letters, v. 373, no. 0, p. 41-53.

Magee, C., Jackson, C. L., and Schofield, N., 2014a, Diachronous sub-volcanic intrusion along deep-water margins: insights from the Irish Rockall Basin: Basin Research, v. 26, no. 1, p. 85-105.

Magee, C., McDermott, K. G., Stevenson, C. T., and Jackson, C. A.-L., 2014b, Influence of crystallised igneous intrusions on fault nucleation and reactivation during continental extension: Journal of Structural Geology, v. 62, p. 183-193.

Magee, C., Duffy, O. B., Purnell, K., Bell, R. E., Jackson, C. A. L., and Reeve, M. T., 2015, Fault-controlled fluid flow inferred from hydrothermal vents imaged in 3D seismic reflection data, offshore NW Australia: Basin Research.

Malthe-Sørenssen, A., Planke, S., Svensen, H., and Jamtveit, B., 2004, Formation of saucer-shaped sills, *in* Breitkreuz, C., and Petford, N., eds., Physical geology of high-level magmatic systems. Geological Society, London, Special Publications, Volume 234, Geological Society, London, Special Publications, p. 215-227.

Mavko, G., Mukerji, T., and Dvorkin, J., 2009, The rock physics handbook: Tools for seismic analysis of porous media, Cambridge university press.

McClay, K., Scarselli, N., and Jitmahantakul, S., 2013, Igneous intrusions in the Carnarvon Basin, NW Shelf, Australia, *in* Keep, M., and Moss, S. J., eds., The Sedimentary Basins of Western Australia IV: Perth, WA, Proceedings of the Petroleum Exploration Society of Australia Symposium.

Morgan, S., Stanik, A., Horsman, E., Tikoff, B., de Saint Blanquat, M., and Habert, G., 2008, Emplacement of multiple magma sheets and wall rock deformation: Trachyte Mesa intrusion, Henry Mountains, Utah: Journal of Structural Geology, v. 30, no. 4, p. 491-512.

Osagiede, E. E., Duffy, O. B., Jackson, C. A.-L., and Wrona, T., 2014, Quantifying the growth history of seismically imaged normal faults: Journal of Structural Geology, v. 66, p. 382-399.

Pagli, C., Wright, T. J., Ebinger, C. J., Yun, S.-H., Cann, J. R., Barnie, T., and Ayele, A., 2012, Shallow axial magma chamber at the slow-spreading Erta Ale Ridge: Nature Geoscience, v. 5, no. 4, p. 284-288.

Planke, S., Rasmussen, T., Rey, S. S., and Myklebust, R., 2005, Seismic characteristics and distribution of volcanic intrusions and hydrothermal vent complexes in the Vøring and Møre basins, *in* Doré, A. G., ed., Petroleum Geology: North-West Europe and Global Perspectives - Proceddings of the 6th Petroleum Geology Conference, Geological Society, London, p. 833-844.

Pollard, D. D., and Johnson, A. M., 1973, Mechanics of growth of some laccolithic intrusions in the Henry Mountains, Utah, II: bending and failure of overburden layers and sill formation: Tectonophysics, v. 18, no. 3, p. 311-354.

Pollard, D. D., Muller, O. H., and Dockstader, D. R., 1975, The form and growth of fingered sheet intrusions: Geological Society of America Bulletin, v. 86, no. 3, p. 351-363.

Polteau, S., Mazzini, A., Galland, O., Planke, S., and Malthe-Sørenssen, A., 2008, Saucer-shaped intrusions: occurrences, emplacement and implications: Earth and Planetary Science Letters, v. 266, no. 1, p. 195-204.

Rickwood, P., 1990, The anatomy of a dyke and the determination of propagation and magma flow directions: Mafic dykes and emplacement mechanisms, p. 81-100.

Rohrman, M., 2013, Intrusive large igneous provinces below sedimentary basins: An example from the Exmouth Plateau (NW Australia): Journal of Geophysical Research: Solid Earth, v. 118, no. 8, p. 4477-4487.

Rubin, A. M., 1995, Propogation of magma-filled cracks: Annual Review of Earth and Planetary Sciences, v. 23, p. 49.

Schofield, N., Stevenson, C., and Reston, T., 2010, Magma fingers and host rock fluidization in the emplacement of sills: Geology, v. 38, no. 1, p. 63-66.

Schofield, N., Heaton, L., Holford, S. P., Archer, S. G., Jackson, C. A. L., and Jolley, D. W., 2012a, Seismic imaging of 'broken bridges': linking seismic to outcrop-scale investigations of intrusive magma lobes: Journal of the Geological Society, v. 169, no. 4, p. 421-426.

Schofield, N. J., Brown, D. J., Magee, C., and Stevenson, C. T., 2012b, Sill morphology and comparison of brittle and non-brittle emplacement mechanisms: Journal of the Geological Society, v. 169, no. 2, p. 127-141.

Schwab, A., Cronin, B., and Ferreira, H., 2007, Seismic expression of channel outcrops: Offset stacked versus amalgamated channel systems: Marine and Petroleum Geology, v. 24, no. 6, p. 504-514.

Sclater, J. G., and Christie, P., 1980, Continental stretching: An explanation of the Post-Mid-Cretaceous subsidence of the central North Sea Basin: Journal of Geophysical Research: Solid Earth (1978–2012), v. 85, no. B7, p. 3711-3739.

Skogly, O., 1998, Seismic characterization and emplacement of intrusives in the Vøring BasinM.Sc. Thesis]: University of Oslo.

Smallwood, J. R., and Maresh, J., 2002, The properties, morphology and distribution of igneous sills: modelling, borehole data and 3D seismic from the Faroe-Shetland area, *in* Jolley, D. W., and Bell, B. R., eds., The North Atlantic Igneous Province:

Stratigraphy, tectonic, Volcanic and Magmatic Processes, Volume 197, Geological Society, London, Special Publications, p. 271-306.

Sun, Q., Wu, S., Cartwright, J., Wang, S., Lu, Y., Chen, D., and Dong, D., 2014, Neogene igneous intrusions in the northern South China Sea: Evidence from high-resolution three dimensional seismic data: Marine and Petroleum Geology, v. 54, p. 83-95.

Svensen, H., Corfu, F., Polteau, S., Hammer, Ø., and Planke, S., 2012, Rapid magma emplacement in the Karoo Large Igneous Province: Earth and Planetary Science Letters, v. 325-326, p. 1-9.

Symonds, P. A., Planke, S., Frey, O., and Skogseid, J., 1998, Volcanic evolution of the Western Australian Continental Margin and its implications for basin development: The Sedimentary Basins of Western Australia 2: Proc. of Petroleum Society Australia Symposium, Perth, WA.

Thomson, K., and Hutton, D., 2004, Geometry and growth of sill complexes: insights using 3D seismic from the North Rockall Trough: Bulletin of Volcanology, v. 66, no. 4, p. 364-375.

Thomson, K., 2005, Volcanic features of the North Rockall Trough: application of visualisation techniques on 3D seismic reflection data: Bulletin of Volcanology, v. 67, no. 2, p. 116-128.

Thomson, K., and Schofield, N., 2008, Lithological and structural controls on the emplacement and morphology of sills in sedimentary basins, *in* Thomson, K., and Petford, N., eds., Structure and Emplacement of High-Level Magmatic Systems, Volume 302, Geological Society, London, Special Publications, p. 31-44.

Widess, M., 1973, How thin is a thin bed?: Geophysics, v. 38, no. 6, p. 1176-1180.

Wright, T. J., Ebinger, C., Biggs, J., Ayele, A., Yirgu, G., Keir, D., and Stork, A., 2006, Magma-maintained rift segmentation at continental rupture in the 2005 Afar dyking episode: Nature, v. 442, no. 7100, p. 291-294.

TABLE 1. MAGMA FINGER FIELD MEASUREMENTS

Location	Width (m)	Height (m)	Ratio	Reference
Golden Valley	500.0	100.00	0.20	Schofield et al. (2012b)
Ardnamurchan	005.4	002.30	0.43	
Raton	005.0	001.00	0.20	
Whin sill	003.0	000.75	0.25	
Shonkin sag (proximal to source)	005.0	002.00	0.40	Pollard and Johnson (1973)
Shonkin sag (distal to source)	003.0	001.20	0.40	
Trachyte Mesa	008.0	001.25	0.16	Morgan et al. (2008)
Trachyte Mesa	010.0	001.25	0.13	

TABLE 2. ROCK PROPERTIES

Rocks	Porosity	Grain density (g cm^{-3})	Bulk density (g cm^{-3})	Matrix bulk modulus (GPa)	Matrix shear modulus (GPa)	Bulk modulus (GPa)	Shear modulus (GPa)	Sonic velocity (km s^{-1})
Igneous	-	-	2.8	-	-	-	-	5.55
Sandstone	0.25	2.65	2.24	36 (Quartz)	45 (Quartz)	7.45	0.60	1.92
Shale	0.18	2.45	2.19	17.8 (Smectite)	4.7 (Smectite)	7.92	0.83	2.03

Figure 1

Click here to download Figure: Fig. 1 - seismic and field examples.pdf

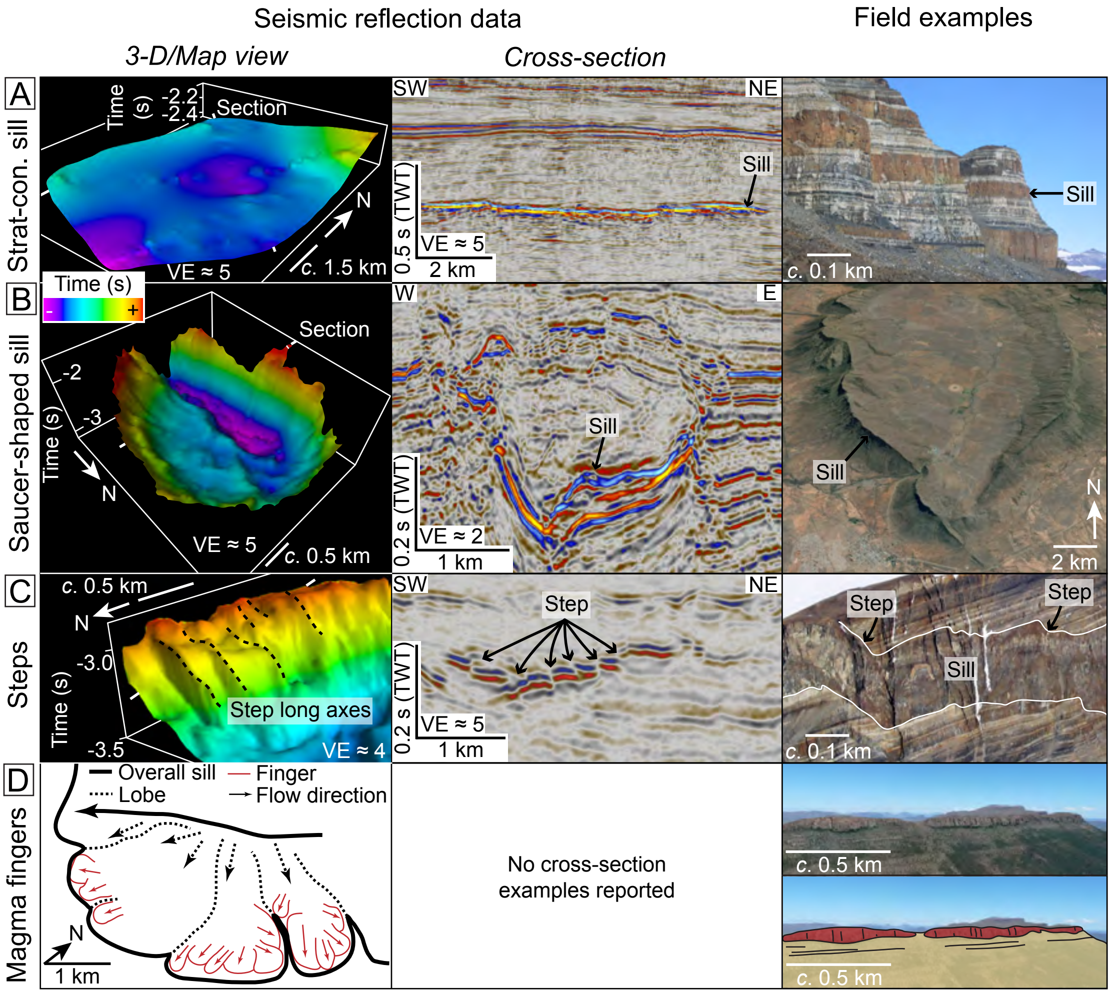

Figure 2
Click here to download Figure: Fig. 2 - input models.pdf

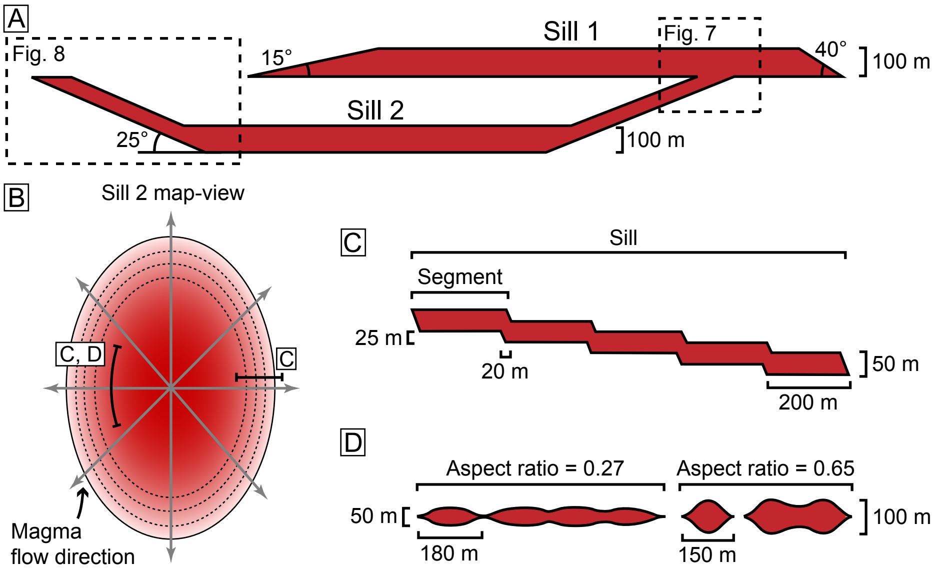

Figure 3
Click here to download Figure: Fig. 3 - Flow indicators.pdf

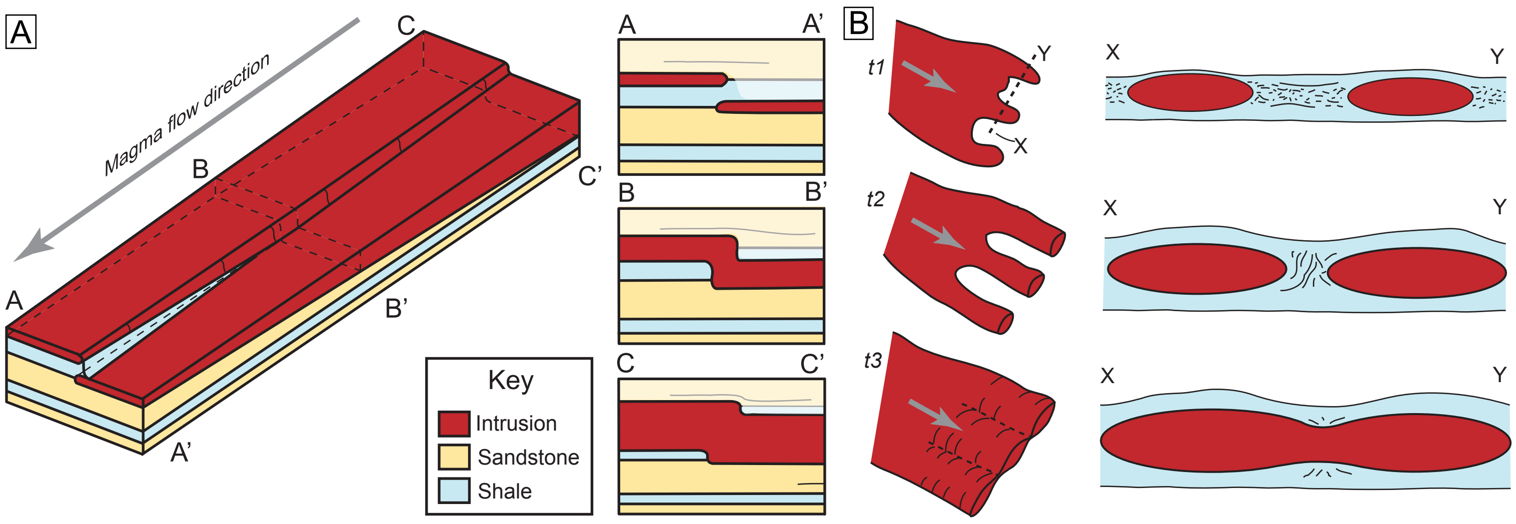

Figure 4

Click here to download Figure: Fig. 4 - Intrusion resolution.pdf

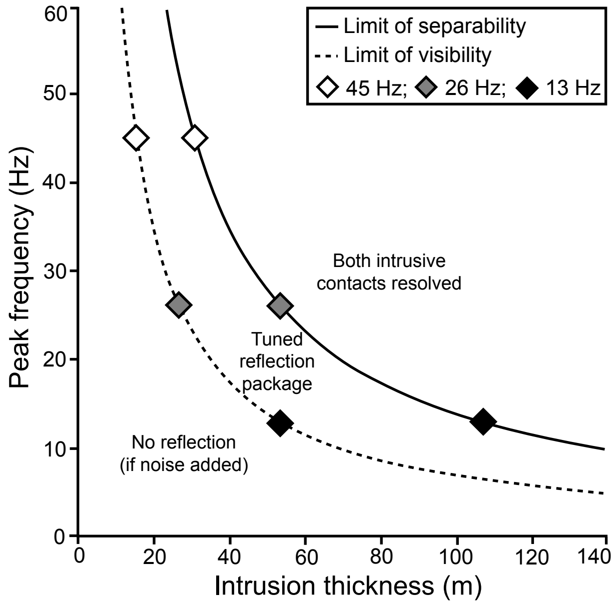

Figure 5
Click here to download Figure: Fig. 5 - Main model homo.pdf

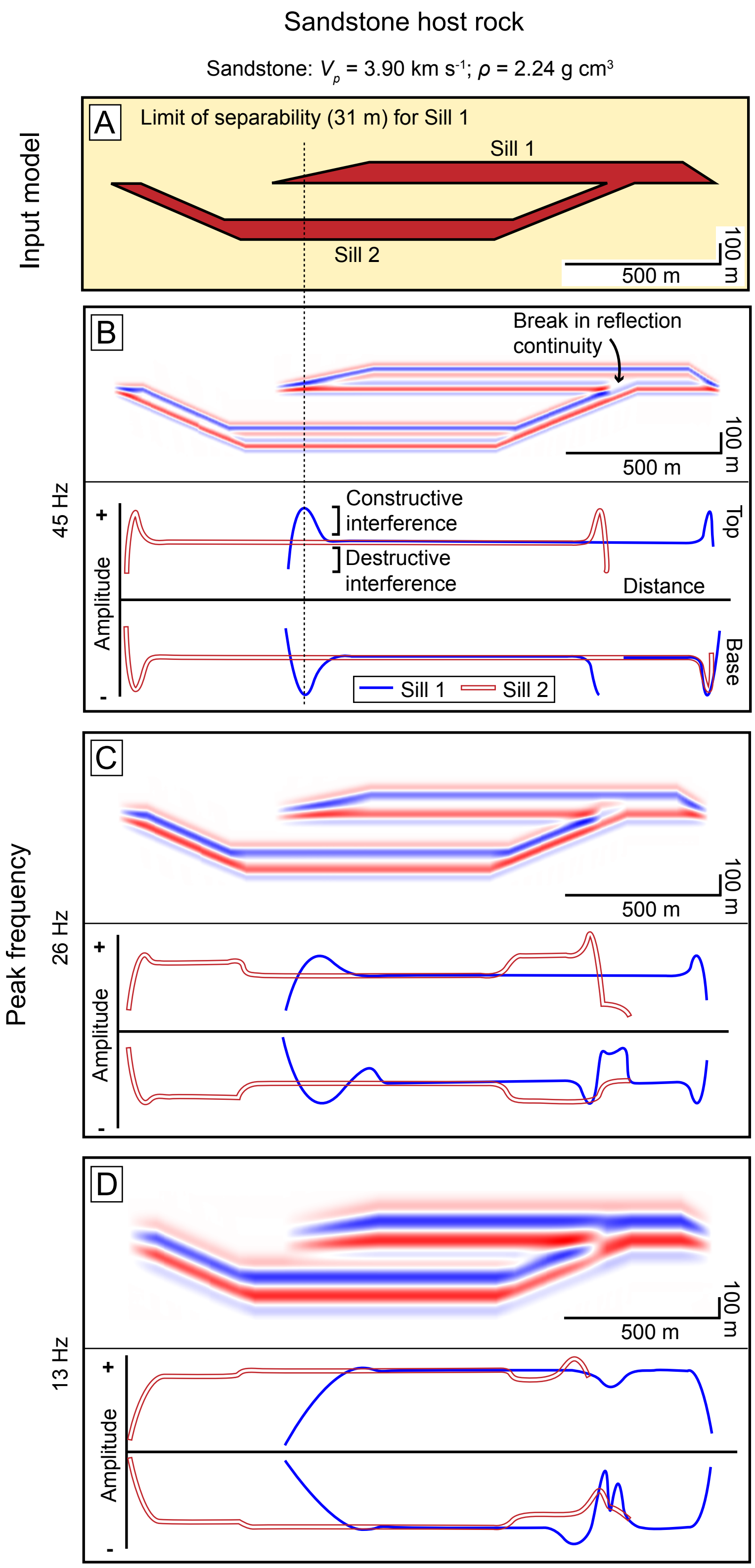

Figure 6
Click here to download Figure: Fig. 6 - Main model.pdf

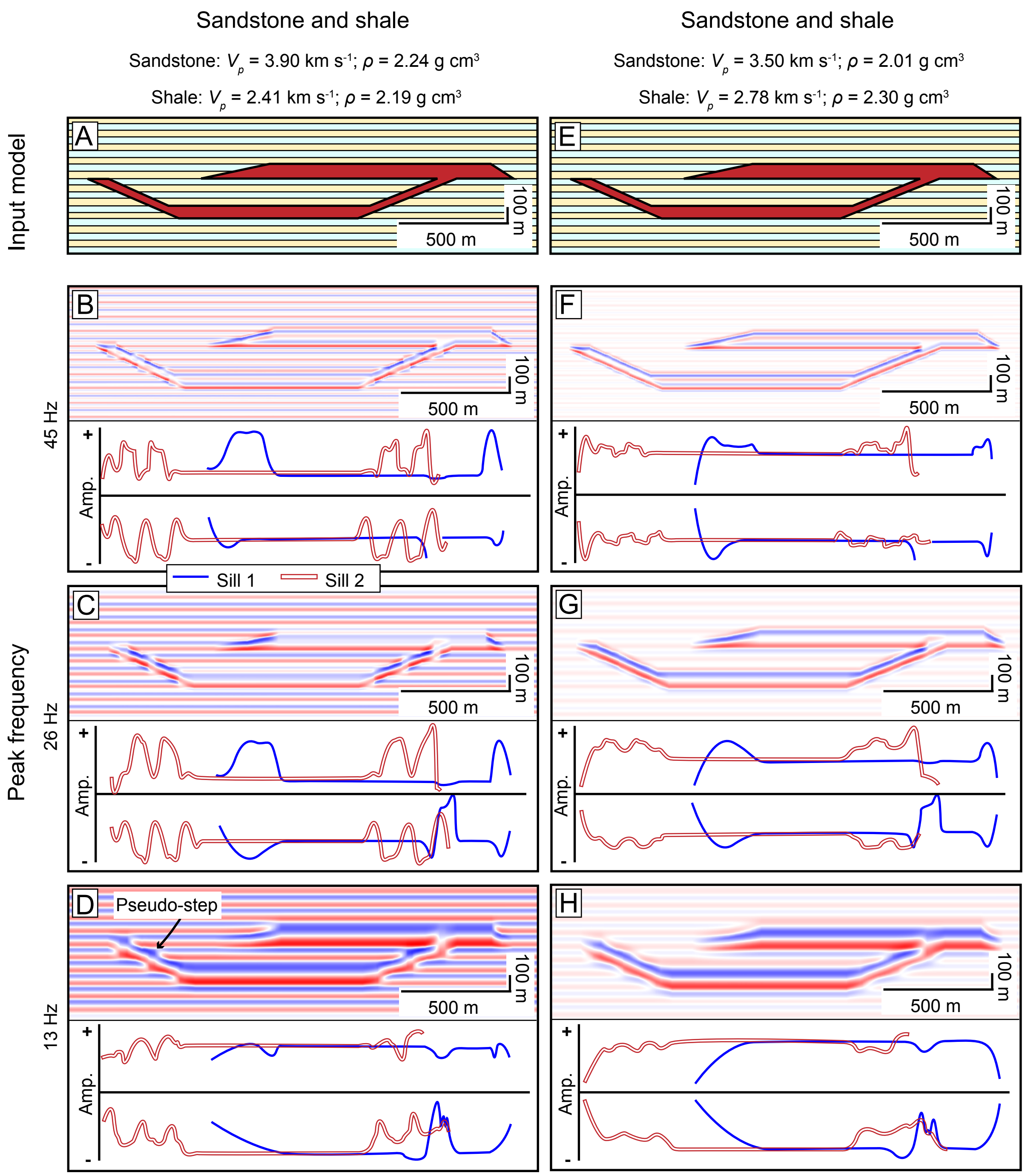

Figure 7
Click here to download Figure: Fig. 7 - Junctions.pdf

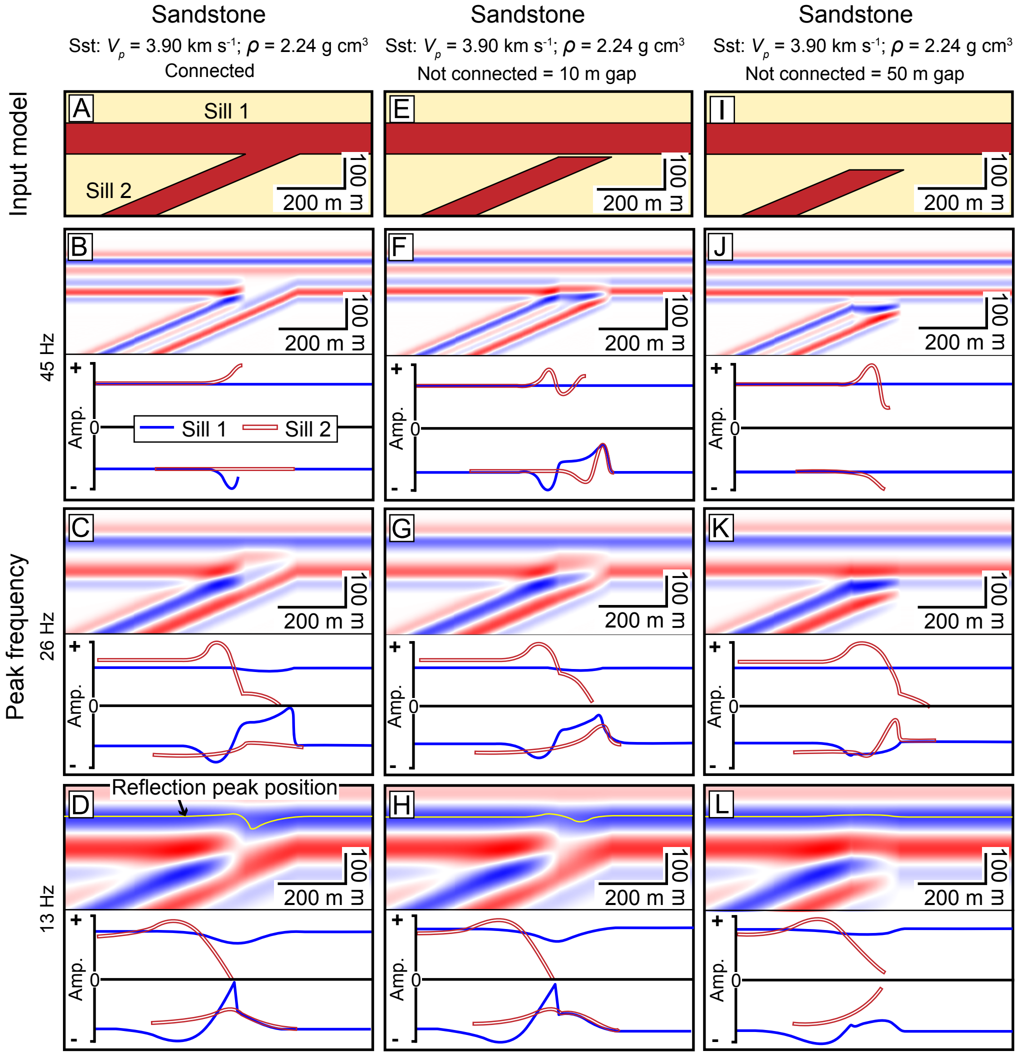

Figure 8
Click here to download Figure: Fig. 8 - inc ramp.pdf

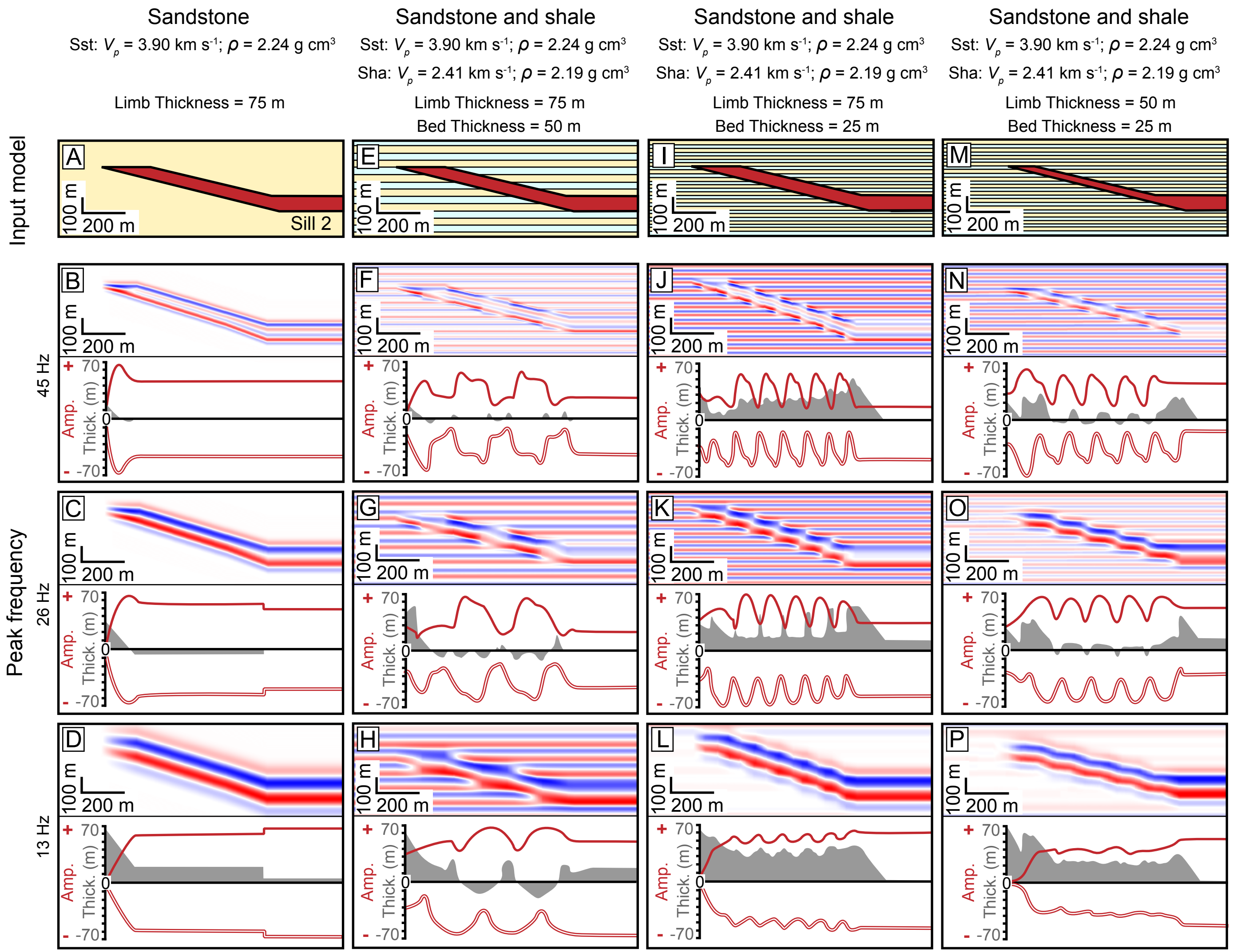

Figure 9

Click here to download Figure: Fig. 9 - step-stair.pdf

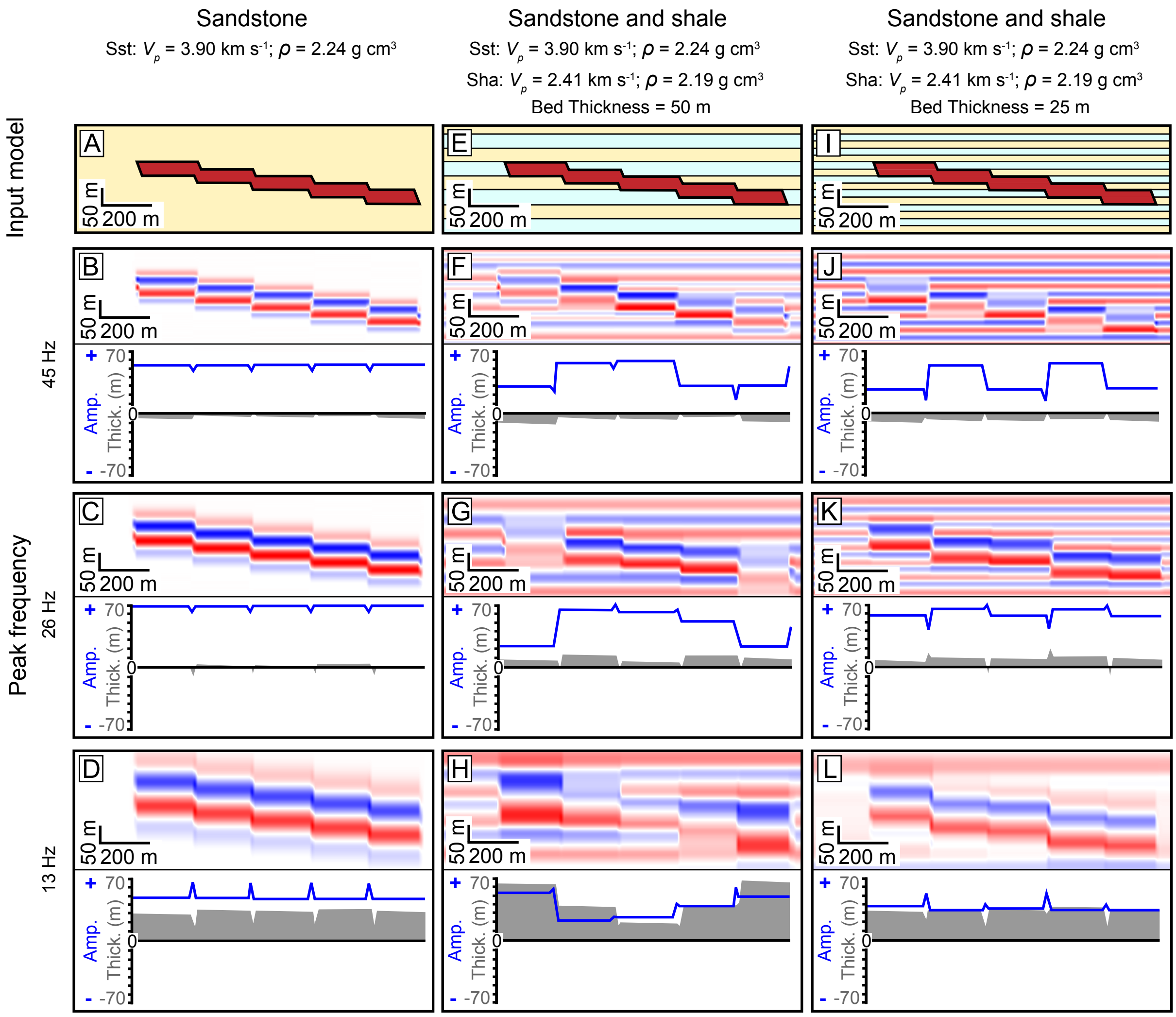

Figure 10

Click here to download Figure: Fig. 10 - fingers.pdf

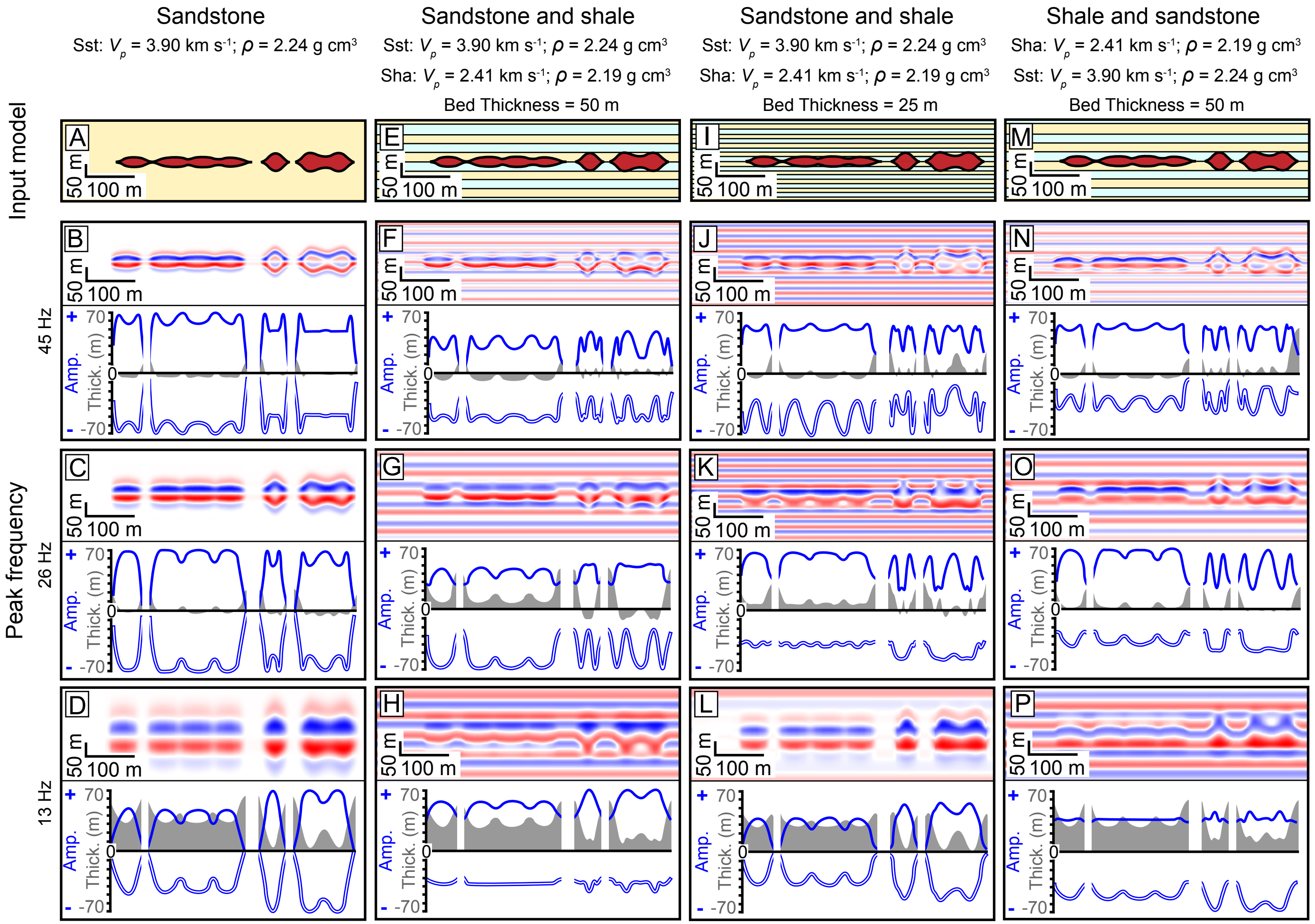

Figure 11
Click here to download Figure: Fig. 11 - sill connection.pdf

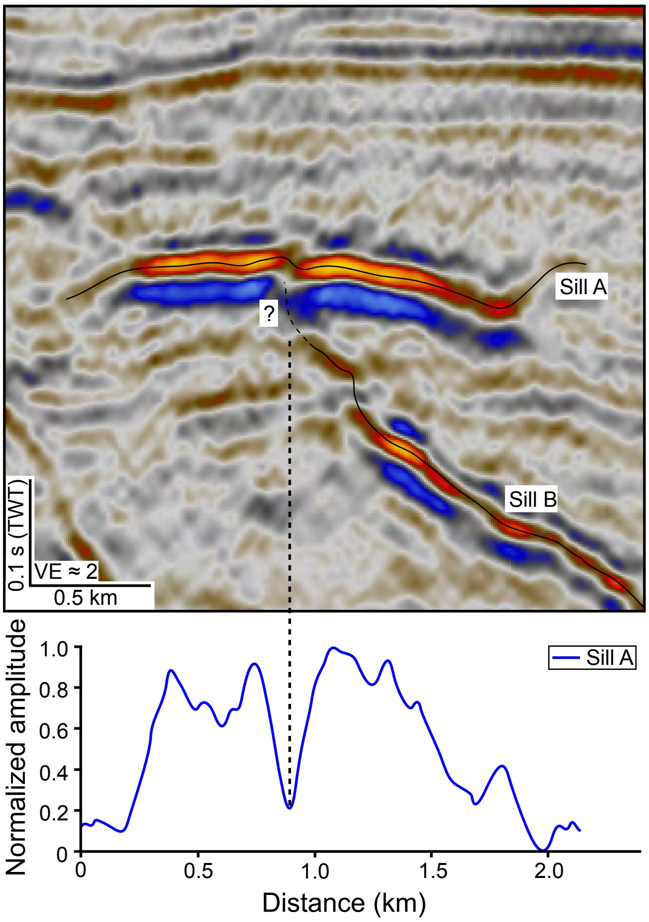

Figure 12

Click here to download Figure: Fig. 12 - Inc sheet formation.pdf

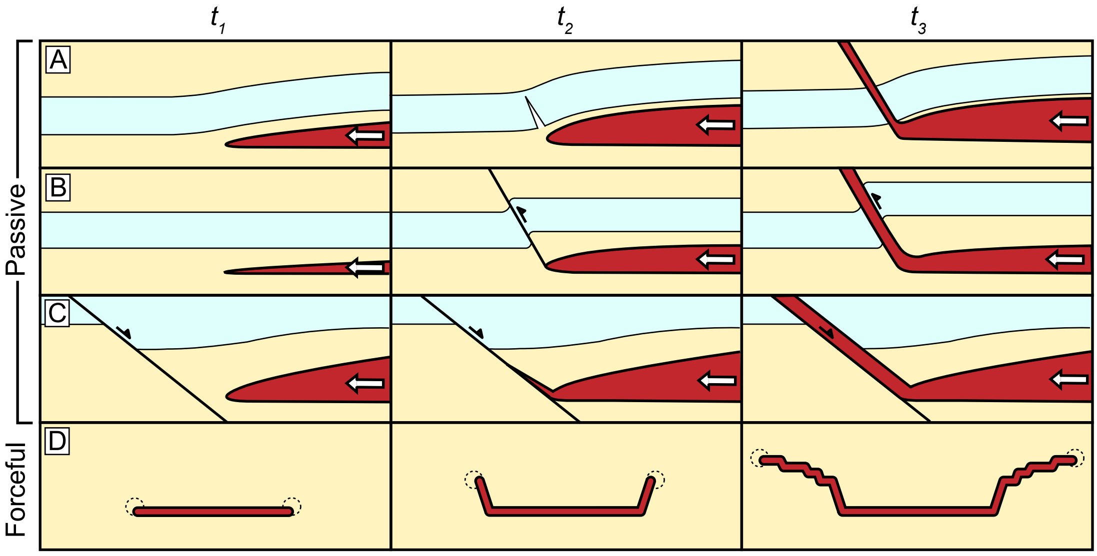

Figure 13

Click here to download Figure: Fig. 13 - inc. sheet tuning wedge.pdf

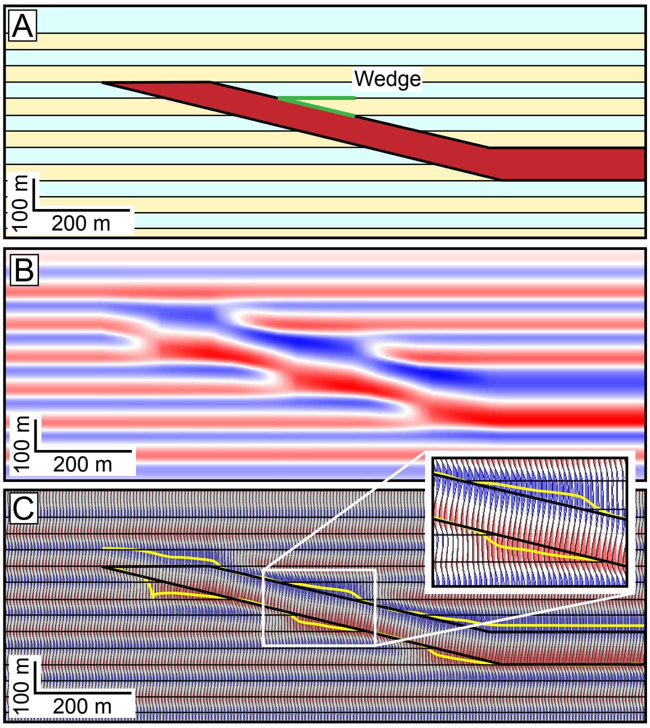

Figure 14

Click here to download Figure: Fig. 14 - inclined limb real.pdf